

Supplemental Figure 1: *C3ar1*^{-/-} mice have an increased inflammatory infiltrate during the more chronic phase of SCI. Note the increase in Iba1 staining (microglia/macrophages; **A**) and also the greater presence of CD3⁺ T cell numbers (**B**) at the site of SCI in *C3ar1*^{-/-} mice (35 days post-injury). Bar graphs are mean ± SEM, with data points representing individual mice for each cohort (n=5-6 per group); *, p<0.05; two-tailed Student's t-test. Scale bars: 15 μm.

Supplemental Figure 2: SCI leads to local and systemic changes in the presence of granulocyte mobilizing/chemotactic factors. Spinal cord (T11-13 segment) and plasma samples were collected from sham and SCI mice at 2 h post-surgery. **A:** Hemoglobin content of spinal cord samples was elevated in response to SCI but not different between WT and

C3ar1^{-/-} mice. **B, C**: C5a levels were similarly increased in the spinal cord (**B**) and plasma (**C**) of WT and *C3ar1*^{-/-} mice after injury. **D**: Surface expression of C5aR1 was elevated on circulating granulocytes in response to SCI, as evident from a significant increase in the median fluorescence staining intensity (MFI), but not different between genotypes. **E, F**: Levels of CXCL1, a potent granulocyte mobilizing/chemotactic factor, were also significantly increased in spinal cord (**E**) and plasma (**F**) following SCI but not different between WT and *C3ar1*^{-/-} mice. **G, H**: G-CSF levels were trending higher in the spinal cord (**G**), and significantly increased in plasma following SCI (**H**). **I**: Plasma CXCL12 (SDF-1 α) levels appeared lower in SCI mice, albeit not significantly reduced compared to their sham-operated counterparts; they were also not different between genotypes. For all graphs, data points are individual mice (n=4-5 per genotype / condition), with lines representing group means \pm SEM; *, p<0.05; **, p<0.01; two-way ANOVA with Bonferroni *post hoc* tests.

Supplemental Figure 3: Influence of genotype and SCI on expression of select chemokine receptors, C5a and BM protease levels. **A, B**: C3aR1 deficiency did not affect surface expression of CXCR2 (**A**) and CXCR4 (**B**) on BM neutrophils (MFI: geometric mean fluorescence intensity). Bar graphs are mean \pm SEM, with data points representing individual mice (n=4 per group). **C**: C5a levels in BM extracellular fluid are unchanged between WT and *C3ar1*^{-/-} mice at comparable time points. **D**: Neutrophil elastase levels were increased in *C3ar1*^{-/-} mice at 24 h post-injury. **E, F**: Cathepsin G levels (**E**) and MMP-9 activity (**F**) in BM extracellular fluid were acutely decreased after SCI, but their overall responsiveness was comparable between genotypes. **C-E**: Data points are mean \pm SEM; n=6 per group; **, p<0.01; two-way ANOVA with Bonferroni *post hoc* tests; **F**: Data points are digested gel volumes (normalized to naïve / uninjured controls) from pooled BM extracellular fluid samples (n=6 mice per time point). **(G)** MMP-9 gel zymography for pooled BM extracellular

fluid samples of WT and *C3ar1*^{-/-} mice under homeostatic (naïve) and SCI conditions. Note that average MMP-9 levels appeared lower in *C3ar1*^{-/-} mice.

Supplemental Figure 4: Impact of early neutrophil depletion on the recruitment of other inflammatory cells during the acute, subacute and intermediate phases of SCI. A, B: Flow cytometry plots of the main gating strategies used to identify various infiltrating immune cell populations (i.e. NK1.1⁺ natural killer (NK) cells, CD45^{hi}CD64^{hi} monocytes/macrophages, B220^{neg}CD11c⁺MHC-II⁺ conventional dendritic cells (cDCs), B220⁺CD11c⁺MHC-II⁺ plasmacytoid DCs, CD3⁺ T cells, CD3⁺CD4⁺ T helper cells, and B220⁺CD11c⁻ B cells) in SCI mice at 1, 7 (A) and 14 (B) days post-injury. C: Relative reduction in the presence of a CD45⁺CD64^{neg/dim}B220^{mid} B cell subset at 1 day post-SCI in α -Ly6G-treated mice. D, E: Confocal images confirming the presence of B220⁺ cells (red; rat anti-mouse B220; Serotec, clone RA3-6B2) at the lesion site during the acute phase of SCI; vasculature (goat anti-mouse CD31; R&D Systems, #AF3628) is shown in green, and cell nuclei are blue (DAPI). F: Relative reduction in the presence of a CD45^{hi}CD64^{hi}CD11b⁺ monocytes/macrophages at 14 day post-SCI in α -Ly6G-treated mice. C, F: Bar graphs are mean \pm SEM, with data points representing individual animals; n=6 per group from 3 independent experimental repeats; *, p<0.05; two-tailed Mann-Whitney U test. Scale bar (in D): 20 μ m.

Supplemental Figure 5: C3aR1 agonism prevents in vitro migration of Ly6G-enriched BM neutrophils towards C5a. WT and *C3ar1*^{-/-} cells showed a comparable chemotactic response to C5a (left); dashed line indicates baseline with no chemoattractant present. *C5ar1*^{-/-} cells did not respond to C5a, indicating that the observed migratory effect was dependent on

C5aR1 presence. Addition of the C3aR1 agonist E7 (10 μ M) to the lower (L) compartment did not induce a chemotactic response (*middle*). Addition of E7 to the upper (U) compartment completely abrogated the migration of WT but not *C3ar1*^{-/-} cells towards C5a (*right*). Lines are group means \pm SEM (n=8-12 per group); *, p<0.05; **, p<0.01; ***, p<0.001; one-way ANOVA with Bonferroni *post hoc* tests.

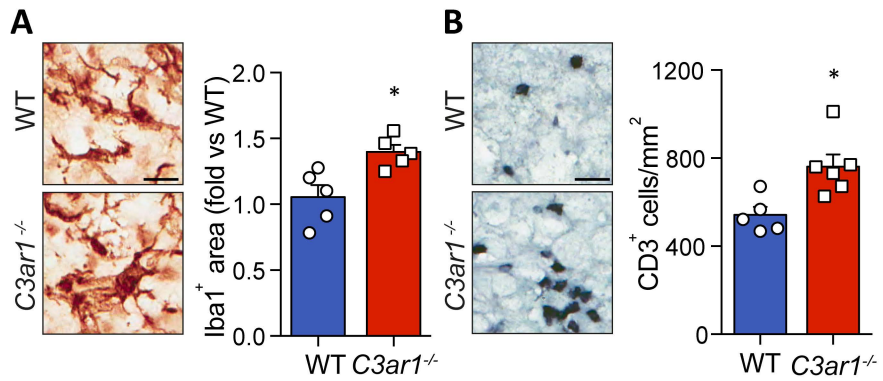
Supplemental Figure 6: Negative regulation of the PI3K/AKT pathway by C3aR1 in human neutrophils. (A) C3aR1 agonism (E7 treatment) leads to ERK1/2 phosphorylation in human peripheral blood neutrophils. (B) IL-8-induced increases in phosphorylated AKT are attenuated by E7 exposure / C3aR1 activation in human peripheral blood neutrophils. Addition of VO-OHpic revealed again that this antagonistic effect of C3aR activation is PTEN-dependent. Data points are biological replicates, with lines representing group means \pm SEM (n=3-4 per condition). **A:** **, p<0.01; two-sided Student's t test; **B:** *, p<0.05; one-way ANOVA with Bonferroni *post hoc* tests.

Supplemental Figure 7: SHP-1 inhibition does not lead to granulocytosis in WT SCI mice. (A) Representative flow cytometry plots and gating strategy for blood samples from WT SCI mice (2 hours post-injury), treated with either PBS or NSC87877 (2.5 mg/kg i.p.). NSC87877 treatment had no bearing on the number of circulating granulocytes (B), monocytes (C), and lymphoid cells (D) in the blood. Granulocyte frequency within the CD11b⁺ population was also unchanged (E). Bars are mean \pm SEM, with data points representing individual mice (n=5 per group); p>0.33, two-sided Student's t test.

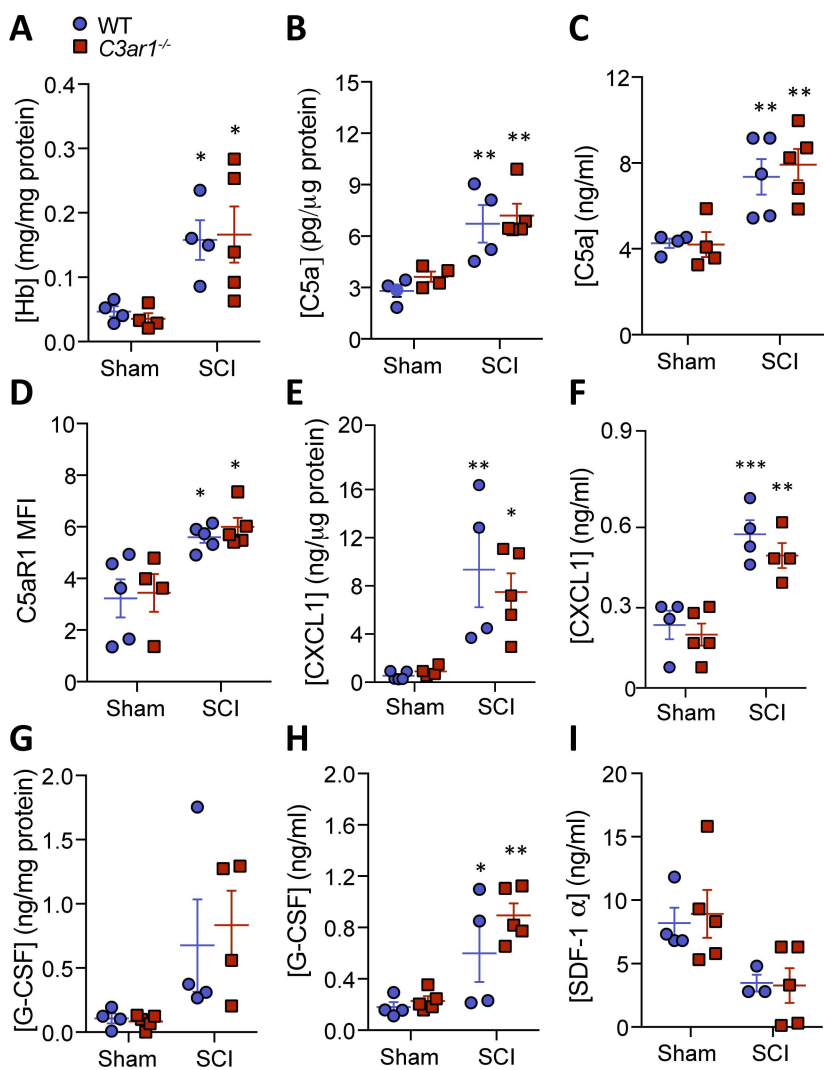
Supplemental Figure 8: Proposed model for how C3aR1 negatively regulates BM neutrophil mobilization in response to tissue injury and systemic inflammation. A: Changes in various mobilizing factors, including C5a and G-CSF but particularly CXCL1, in

the bone marrow (BM) niche promote the release of granulocytes into the circulation. Mobilized Ly6G⁺ neutrophils migrate to the spinal cord lesion site, where they contribute to neuroinflammatory processes and cause secondary injury. CXCL12 and C3a promote the retention of neutrophils within the BM via their respective receptors, CXCR4 and C3aR1. This negatively regulates the magnitude of the peripheral inflammatory response to SCI. ROS: reactive oxygen species, MPO: myeloperoxidase. **B:** C3aR1 controls BM neutrophil mobilization / migration via PTEN and its negative regulatory influence over the PI3K/AKT pathway.

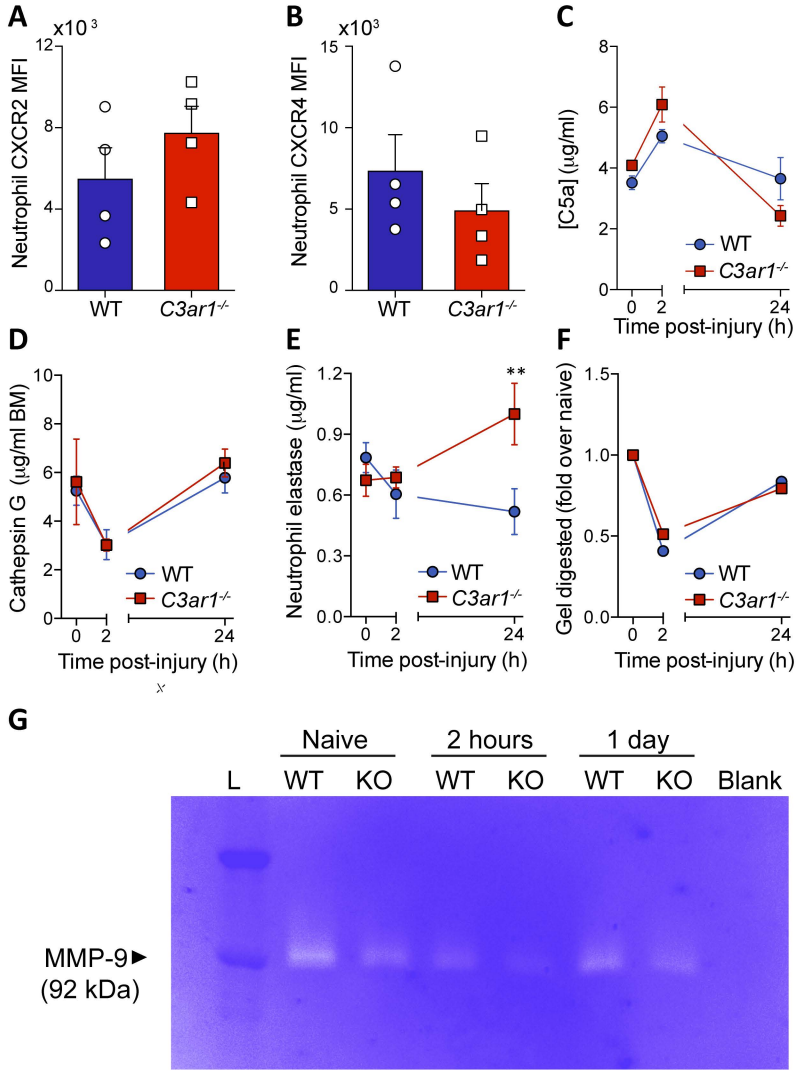
SUP FIGURE 1



SUP FIGURE 2

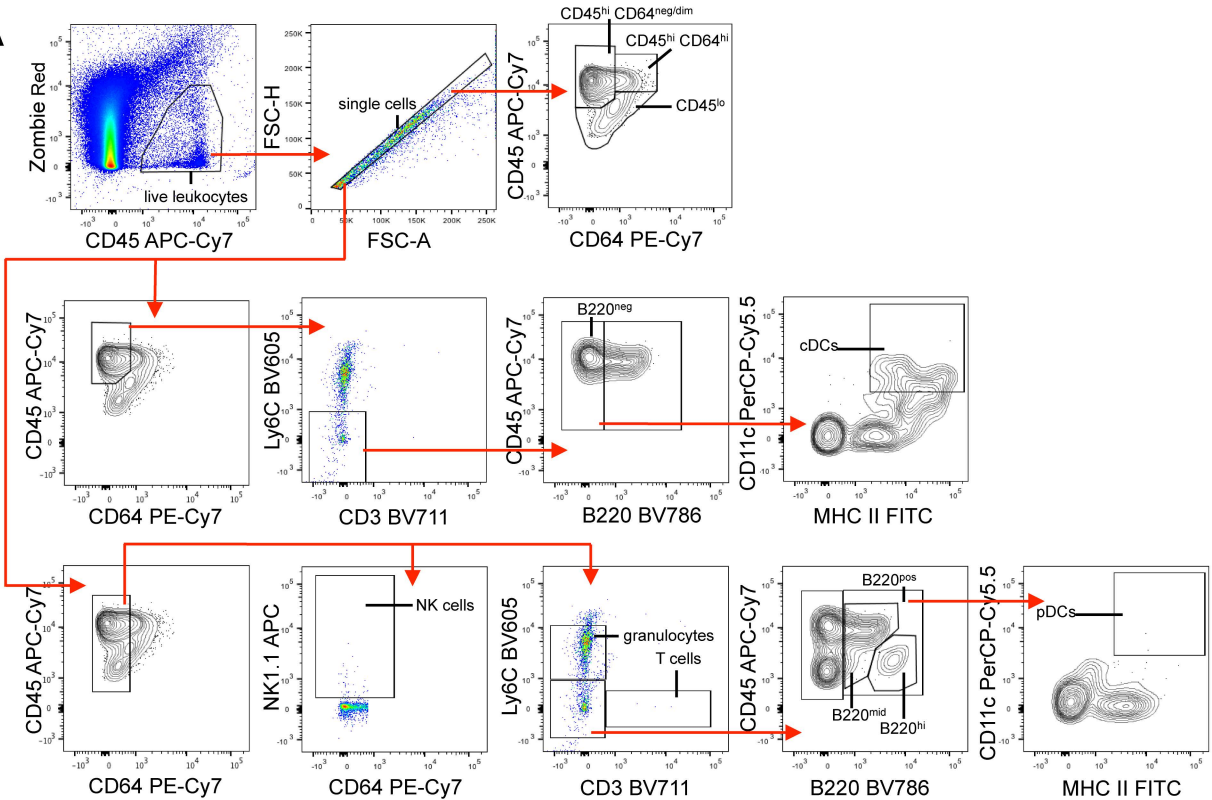


SUP FIGURE 3

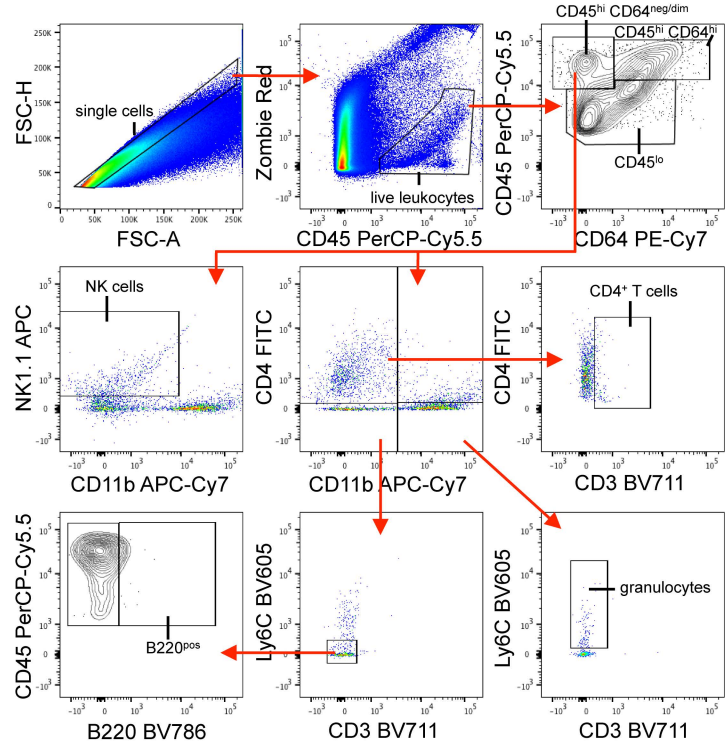


SUP FIGURE 4

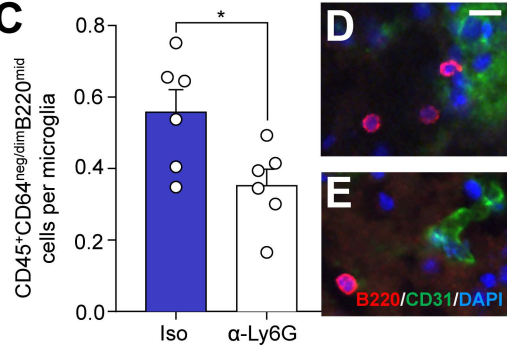
A



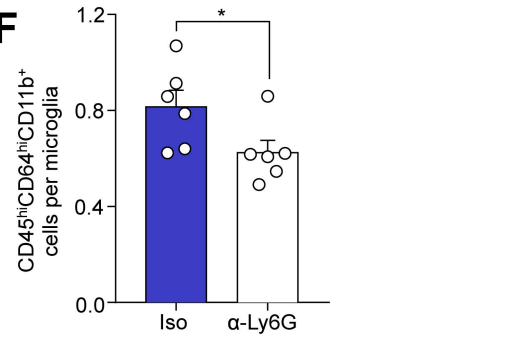
B



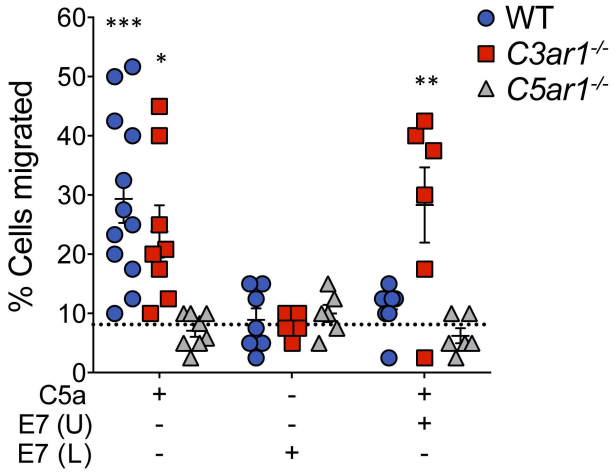
C



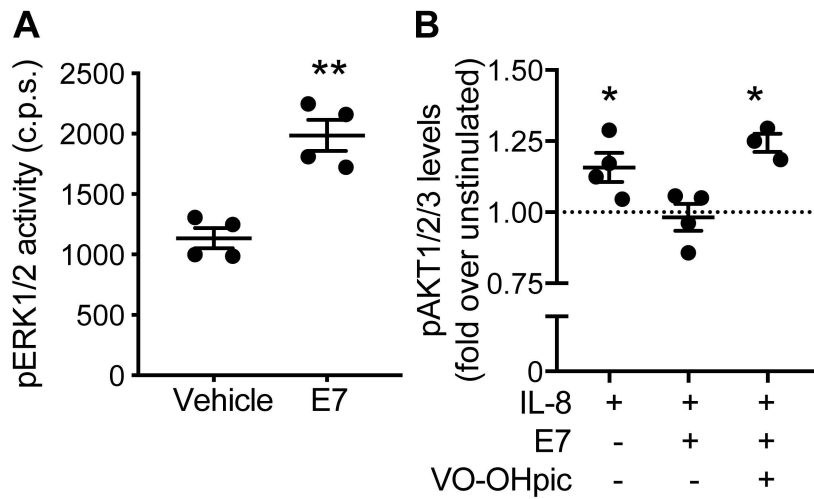
F



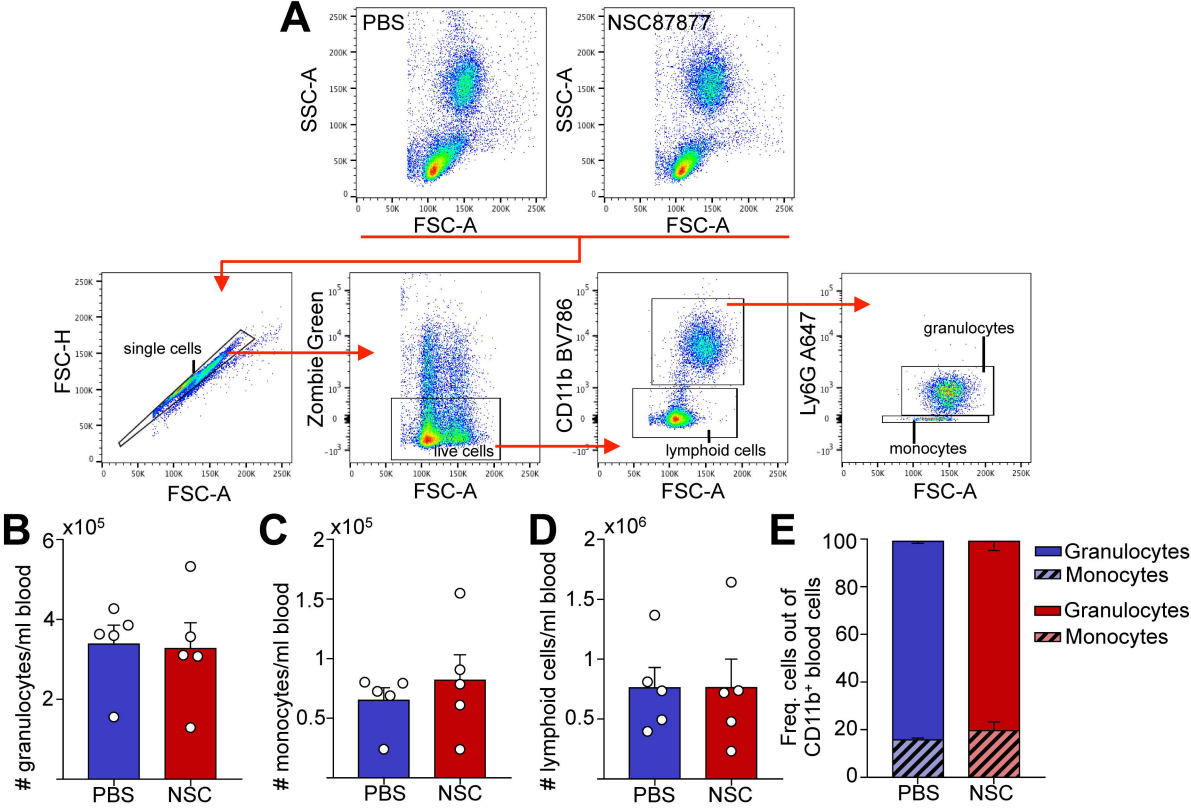
SUP FIGURE 5



SUP FIGURE 6



SUP FIGURE 7



SUP FIGURE 8

